First principles study of post-boron carbide phases with icosahedra broken*

Ming-Wei Chen(陈明伟), Zhao Liang(梁钊), Mei-Ling Liu(刘美玲),
Uppalapati Pramod Kumar, Chao Liu(刘超)†, and Tong-Xiang Liang(梁彤祥)‡

Faculty of Materials Metallurgy and Chemistry, Jiangxi University of Science and Technology, Ganzhou 341000, *China*

(Received 18 March 2020; revised manuscript received 11 June 2020; accepted manuscript online 29 June 2020)

Boron carbide (B_4C) is a rhombic structure composed of icosahedra and atomic chains, which has an important application in armored materials. The application of B_4C under super high pressure without failure is a hot spot of research. Previous studies have unmasked the essential cause of B_4C failure, *i.e.*, its structure will change subjected to impact, especially under the non-hydrostatic pressure and shear stress. However, the change of structure has not been clearly understood nor accurately determined. Here in this paper, we propose several B_4C polymorphs including B_4C high pressure phases with non-icosahedra, which are denoted as post-B_4C and their structures are formed due to icosahedra broken and may be obtained through high pressure and high temperature (HPHT). The research of their physical properties indicates that these B_4C polymorphs have outstanding mechanical and electrical properties. For instance, aP10, mC10, mP20, and oP10-B_4C are conductive superhard materials. We hope that our research will enrich the cognition of high pressure structural deformation of B_4C and broaden the application scope of B_4C.

Keywords: boron carbide, structural transformation, icosahedra broken, physical properties, first principles

PACS: 31.15.E–, 61.50.Ks, 71.20.–b, 91.60.Gf **DOI:** 10.1088/1674-1056/aba097

1. Introduction

Boron carbide (B_4C), as the third hardest material next to diamond and cubic boron nitride, has remarkable mechanical properties such as large elastic moduli including bulk modulus, shear modulus and Young's modulus,[1,2] large fracture toughness and flexure strength,[1,3,4] high hardness,[3–5] high Hugoniot elasitc limit (HEL 15 GPa–20 GPa),[6] which make B_4C possess numerous applications in military and industry areas, with the B_4C serving as tank armor, bulletproof vests, wear-resistant, and cutting tool material, *etc*.[7–9]

However, experimental dynamics on B_4C shows that its resistance against higher velocity threats was severe discounted.[10–12] For the dynamic impact study, the B_4C lost its shear strength as the shock stress exceeded its HEL due to a probable phase transition,[13,14] or amorphization.[8,15] And under shock compression and decompression, a macroscopic slip system plays an important role in the transition of B_4C,[16] and the shear localization band is intimately connected with shear amorphization.[17] With regard to the static stress, there was no phase transition nor amortization observed during compressing the B_4C through diamond anvil cell (DAC) with the hydrostatic pressure until 126 GPa.[18–20] Amorphization or phase transition depends strongly on degree of non-hydrostatic pressure in DAC,[21,22] or scratching and nanoindentation.[23–26] The amorphization of B_4C is associated with the destruction of the C–B–C chains, sp^2-bonded aromatic carbon clusters formed and amorphous boron clusters created by dynamic indentation.[25,26]

Previous studies have pointed that the bending of the chain with the intermediate atoms of the chain bonding to the adjacent icosahedral atoms plays a very dominant role in the stress-induced amorphization of B_4C, and the icosahedra appear more stable than the linear chain under high pressures.[27] However a direct evidence has proved that the formation of amorphous shear bands in B_4C results from the disassembly of the icosahedra during shear deformation.[28] And actually, the icosahedra are less stable than the chains, and the chain–icosahedron bonds are unexpectedly strong,[29] which corroborates the hypothesis suggested by previous QM simulations that the chain–icosahedron interactions trigger shear amorphization.[30]

To figure out the failure of B_4C, the structure evolution has also been surveyed via theoretical research. The Gibbs free energy calculations has revealed that the collapse of B_4C leads B_{12} to be segregated from amorphous carbon,[15] which is in excellent agreement with recent TEM results presented by Chen *et al*.[8] First-principles simulations reveal that the

*Project supported by the National Natural Science Foundation of China (Grant Nos. 51871114 and 12064013), the Natural Science Foundation of Jiangxi Province, China (Grant No. 20202BAB214010), the Research Foundation of the Education Department of Jiangxi Province, China (Grant Nos. GJJ180433 and GJJ180477), the Open Funds of the State Key Laboratory of Metastable Materials Science and Technology, Yanshan University, China (Grant No. 201906), the Ganzhou Science and Technology Innovation Project, China (Grant No. 201960), and the Jiangxi University of Science and Technology Scientific Research Starting Foundation, China (Grant No. jxxjbs17053).

†Corresponding author. E-mail: liuchao198967@126.com

‡Corresponding author. E-mail: liang_tx@126.com

depressurization amorphization results from pressure-induced irreversible bending of C–B–C atomic chains cross-linking 12-atom icosahedra at the rhombohedral vertices.[22]

It is known through studying the mechanism for amorphization of B_4C under uniaxial compression that the B_4C becomes amorphous at a uniaxial strain 0.23, with its maximum stress being 168 GPa. The amorphous state is the consequence of structural collapse associated with the bending of the three-atomic chain, and the B_4C may collapse under a much smaller shear strain (stress) than the uniaxial strain (stress).[31,32] Then An *et al.*,[30] and An and Goddard[33] found that the lowest shear strength slip system $(01\bar{1}\bar{1})/(\bar{1}101)$ brings about a deformation in which B in the CBC chain bonds to C in the icosahedron and then triggers the destruction of this icosahedron, which leads to negative pressure and cavitation, resulting in crack opening and then B_4C material failure.

Although no amorphous phenomena were observed from the B_4C under hydrostatic pressure, theoretically the research gives a unique insight.[34,35] Under hydrostatic stress up to 70 GPa, the C–B–C chain can be bent reversibly, however, non-hydrostatic stress abruptly manifests reversible bending, which facilitates the displaced central B atom in the chain and the atoms in the nearby icosahedra forming weak bonds, with the structure being disordered.[34,35]

In 2017, Zhang *et al.* reported a B_4C polymorphs with $P3_221$ space group (denoted as rH15), which is the high-pressure stable phase with triatomic rings rather than icosahedron. While the rH15 is unstable at ambient pressure.[36] Previous studies have unmasked the essential cause of B_4C failure: its structure will change subjected to impact, especially under the non-hydrostatic pressure and shear stress. However, the change of structure has not been clearly understood nor accurately determined. In this paper, we propose several B_4C polymorphs including a kind of B_4C high-pressure phase with non-icosahedra, which may be obtained through B_4C under high pressure. We study the physical properties of the structure after deformation, and the relationship between physical properties and pressure. This research will enhance the cognition of high-pressure structural deformation of B_4C.

2. Computational methods

The structural search for B_4C polymorphs has been performed in the crystal structure analysis by particle swarm optimization (CALYPSO) code,[37,38] which has been successfully applied to the search for superhard materials.[39] The structural relaxations were implemented in the CASTEP code by using generalized gradient approximation (GGA) in the frame of density functional theory (DFT).[40] The local exchange-correlation functional in CASTEP is PBESOL.[41] To give well converged total energy of 1 meV, the plane-wave basis set with an energy cutoff of 310 eV was adopted, with the ultrasoft pseudopotential and k-points separation ($2\pi \times 0.04$ Å^{-1}) being assigned to generate a k-point grid through using the Monkhorst–Pack grid parameters. During the calculation of elastic constants, the maximum strain amplitude was 0.3% and the calculation was carried out in nice steps for each strain. In order to obtain precise electrical properties, the hybrid functional HSE06 was employed to calculate the electronic band structure and density of states.[42] Other specific parameters not mentioned above are set to be of ultrafine quality.

3. Results and discussion

3.1. Optimization of crystal structures

Experimental research reveals that B_4C is mainly composed of po-B_4C, which has also been verified theoretically.[27,43–45] As shown in Fig. 1(a), the po-B_4C consists of C–B–C chains and $B_{11}Cp$ icosahedra. The other common structures of B_4C are eq-B_4C (C–B–C chains and $B_{11}Ce$ icosahedra) and ch-B_4C (C–C–C chains and B_{12} icosahedra).[27] Like po-B_4C, the cP30 is of icosahedron (B_{12}), and four B_{12} icosahedra are connected with one C atom as shown in Fig. 1(b). In fact, the icosahedral configuration is the result of a tendency for three-centered covalent bonds due to deficiency of valence electrons.[46]

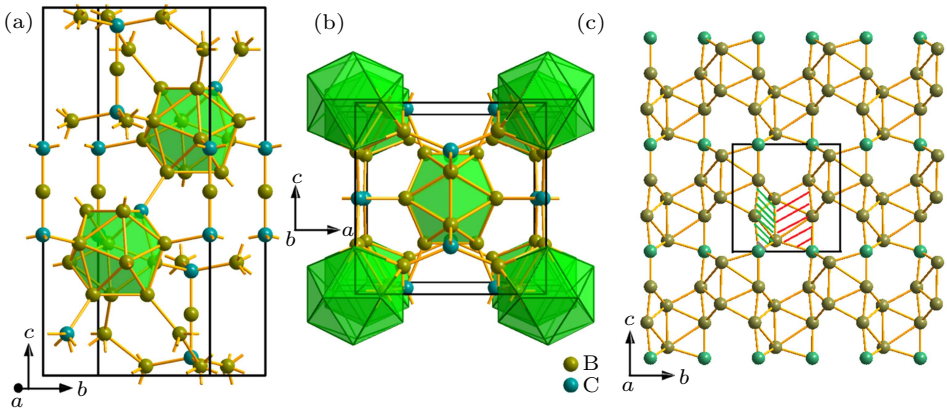

Fig. 1. Structural models for (a) po, (b) cP30, and (c) oP10.

According to the structural searching of CALYPSO and DFT research, several B_4C polymorphs are predicted. Based on information such as about the crystal system, lattice type and the number of atoms contained in the unit cell, these structures are named Pearson symbols. However, none of all the other discovered B_4C polymorphs has icosahedra, but has three-centered covalent bonds. It is an unusual phenomenon for boron-rich materials. For example, oP10, displayed in Fig. 1(c), is connected by five-atomic structural units sharing one vertex or edge. In fact, these structural units are comprised three triangles with the three-centered covalent bonds. Especially, mC10-B_4C (Fig. S1(a) in Supporting information) is C linked borophene, and can be viewed as a sandwich structure formed by alternating layers of B and C. In fact, it is clearly seen that mC10-B_4C is a three-dimensional structure comprised of five-atomic units, which are combined by sharing a vertex or an edge. And the other B_4C polymorphs are exhibited in Figs. S1(b)–S1(f). All the structural information is listed in Table S1. At ambient pressure, the predicted B_4C polymorphs all have higher densities than the B_4C with icosahedra (po, 2.554 g/cm^3, and cP30, 2.645 g/cm^3).

3.2. Stability analysis

According to the Born elastic stability criteria in various crystal systems,[47]
for cubic crystal system:

$$C_{44}>0;\quad C_{11}-C_{12}>0;\quad C_{11}+2C_{12}>0; \tag{1}$$

for hexagonal crystal system:

$$\begin{aligned} &C_{ii}>0;\ \ (i=4,6);\quad C_{11}>|C_{12}|;\\ &2C_{13}^2<C_{33}(C_{11}+C_{12}); \end{aligned} \tag{2}$$

for tetragonal $(4/m)$ crystal system:

$$\begin{aligned} &C_{44}>0;\quad C_{11}>|C_{12}|;\\ &2C_{13}^2<C_{33}(C_{11}+C_{12});\quad 2C_{16}^2<C_{66}(C_{11}-C_{12}); \end{aligned} \tag{3}$$

for orthorhombic crystal system:

$$\begin{aligned} &C_{ii}>0;\quad (i=1,4,5,6);\quad C_{11}C_{22}>C_{12}^2;\\ &C_{11}C_{22}C_{33}+2C_{12}C_{13}C_{23}-C_{11}C_{23}^2-C_{22}C_{13}^2-C_{33}C_{12}^2>0; \end{aligned} \tag{4}$$

for rhombohedral $(\bar{3}m)$ crystal system:

$$\begin{aligned} &C_{44}>0;\quad C_{11}>|C_{12}|;\quad C_{13}^2<0.5C_{33}(C_{11}+C_{12});\\ &C_{14}^2<0.5C_{44}(C_{11}-C_{12})\equiv C_{44}C_{66}. \end{aligned} \tag{5}$$

For low-symmetry system as triclinic and monoclinic, all eigenvalues of the stiffness matrix should be positive.[47]

The calculated values of independent C_{ij} of rH15, tP15, hP20, cP20, and cP30 are listed in Table S2, the simplest form of elastic matrices for aP10, mC10, mP20, and oP1 are displayed below. According to the criteria, all newly discovered B_4C polymorphs with rH15 are mechanically stable at ambient pressure.

Furthermore, the curves of calculated ground state phonon dispersion and the phonon density of states (Fig. S2) of for newly discovered B_4C polymorphs show no imaginary frequency in whole Brillouin zone, indicating their dynamic stability in ambient condition. These results confirm that these B_4C polymorphs are metastable phases in ambient condition. Here, the rH15 B_4C is also studied, and the imaginary frequency indicates that it is unstable at ambient pressure, which is in accordance with the result reported by Zhang *et al.*[36] The phonon dispersion curves and the phonon density of states of po-B_4C are also investigated at ambient pressure. As shown in Fig. S3(a), there is no imaginary frequency, which verifies the dynamic stability of po-B_4C. Meanwhile, the curves of phonon dispersion and the phonon density of states of po-B_4C at high pressure (150 GPa) are studied and displayed in Fig. S3(b). The obvious imaginary frequency indicates that the po-B_4C may go through structural deformation under high pressure.

3.3. Phase transformation under pressure

The relationship between relative enthalpy and pressure for B_4C polymorphs is investigated and displayed in Fig. 2. Here the reported high-pressure phase rH15-B_4C with boron channel-based structure is studied.[36] The ambient-pressure stable phase po-B_4C first transforms to rH15-B_4C at 83.7 GPa, which is consistent with the reported phase transformation, however, smaller than the reported value 96 GPa.[36] Their difference may be caused by the difference in computational method including the exchange-correlation potential, energy cutoff, *etc*. With the pressure increasing, all discovered B_4C polymorphs become more stable than the po-B_4C. In other words, they are all postB_4C phases whose structures are transformed due to icosahedra broken. As is well known, the rH15 can be stable only at a certain high pressure, even if it can be stable at ambient pressure, the predicted oP10, mC10, and aP10 have more advantageous energy than rH15, and the mP20 has the comparable energy with rH15. The other polymorphs including cP20, hP20, and tP15 with high symmetry may exist as metastable phases.

The phonon dispersion spectra and phonon density of state of several B_4C polymorphs at a certain high pressure such as 150 GPa are investigated. As shown in Fig. S4, the phonon dispersion spectra of these B_4C polymorphs with high symmetry including cP30, cP20, and hP20 reveal that there are imaginary frequency, which indicates that these structures become "soft" and tend to be transformed at 150 GPa. However, the other B_4C polymorphs with low symmetry all maintain their

structural stability due to the fact that there is no imaginary frequency but only the maximum vibration frequency of phonon spectrum which increases with pressure increasing. As for rH15, it is dynamically instable at ambient pressure due to the existence of imaginary frequency, while it is dynamically stable at 150 GPa.

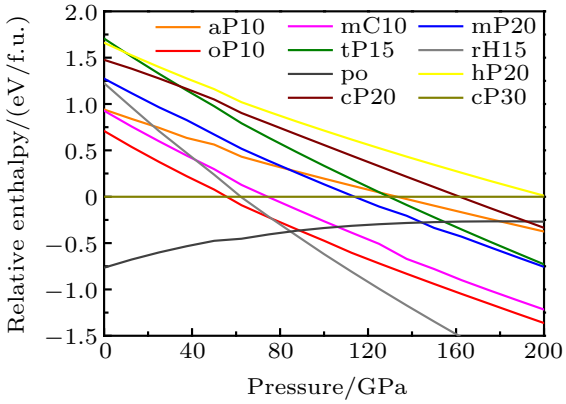

Fig. 2. Curves of enthalpy (relative to cP30) *versus* pressure for various B_4C polymorphs.

It is similar to B that the stable phase at ambient pressure is α-B within B_{12} isosahedon,[44] the first high pressure phase is γ-B (19 GPa–89 GPa) consisting of icosahedral B_{12} clusters and B–B pairs in a NaCl-type arrangement.[48,49] With pressure increasing, the icosahedral B_{12} clusters are replaced by crinkled B layers consisting of B–B–B triangles, the crinkled B layers are connected by B–B covalent bonds, and then the second high pressure phase (α-Ga type B above 89 GPa) is formed.[48,50] The α-B$\rightarrow$ γ-B$\rightarrow$ α-Ga-B phase transformation reveals that the B_{12} icosahedra will collapse and form B3 triangles under rigorous pressure condition. As shown in Fig. S5, the five-atom (four kinds of B atoms and one C atom) units in oP10-B_4C are similar to that of γ-B28,[48] which is composed of one B1atom, two B2 atoms and two B3 atoms, and marked by red lines. Extreme condition like high pressure and high temperature (HPHT), provides tremendous energy to overcome the reaction energy barrier and obtain the metastable phase. The recent study of d-BC_5 indicates that it has metastable character in a relatively narrow temperature range ($\sim$ 200 K) and can be synthesized at 24 GPa and about 2200 K.[51] Under HTHP, the central B atom in the C–B–C chain form bonds to B atoms in the nearby icosahedra accompanied by the chain disappearing and new 3-atom triangles forming. Accompanied with the $B_{11}C$ icosahedra fragmentizing, the five-atom structural units of oP10-B_4C form. So, the oP10-B_4C is very likely obtained through HPHT technology, like the γ-B28 and d-BC_5 that are achieved through the HPHT. Inspired by the atomically thin, crystalline two-dimensional boron sheets can be synthesized atomically thin by molecular beam epitaxy (MBE),[52] and the similarity between boron layers in oP10-B_4C and boron sheets, oP10-B_4C film may be synthesized by the MBE.

3.4. Mechanical properties

The physical properties of B_4C, especially the mechanical properties, deserve extensive attention. Here we investigate the mechanical properties including bulk modulus B, shear modulus G, Young's modulus E, Poisson's ratio ν, and Vickers hardness H_v for each of three commom B_4C phases (ch, eq, and po) with the newly discovered polymorphs. Based on the calculated independent C_{ij}, the mechanical moduli (B, G, E) and Poisson's ratio ν are easy to be determined.[53] And then the values of H_v are solved based on improved empirical formula[54,55]

$$H_v = 0.92\kappa^{1.137}G^{0.708} \quad \text{with} \quad \kappa = G/B. \tag{6}$$

All the calculated physical properties of various B_4C polymorphs are listed in Table 1. The hardness value of po-B_4C is in good agreement with the measured value 30.7 GPa.[5] Among all the discovered B_4C polymorphs, aP10, mC10, mP20, oP10, tP15 are all superhard B_4C polymorphs, mC10-B_4C is the hardest phase, 54.8% higher than the hardness of po-B_4C. The mP20 and tP15 are only a little bit higher than the thresholds for superhard materials. However, cP30 and hP20 have the low hardness, with a value not exceeding 10 GPa, only one-quarter of the hardness of po-B_4C actually.

Table 1. B, G, E, ν, and H_v (in units of GPa) for various B_4C polymorphs at ambient pressure.

	B	G	E	ν	H_v
po	239.44	196.75	463.34	0.177	30.97
aP10	215.39	225.17	500.95	0.112	44.80
mC10	275.33	271.75	613.43	0.129	47.94
mP2	278.80	250.26	577.87	0.155	40.60
oP1	261.14	252.88	573.52	0.134	44.59
tP15	215.21	214.36	482.79	0.126	40.95
hP20	290.18	102.36	274.78	0.342	7.45
cP20	230.97	147.31	364.46	0.237	18.92
cP30	284.03	109.17	290.32	0.330	8.60

Table 2. Values of B, G, E, ν, and H_v (in units of GPa) for various B_4C polymorphs at high pressure of 150 GPa.

	B	G	E	ν	H_v
aP10	704.36	361.12	925.24	0.281	27.84
mC10	728.72	456.61	1133.15	0.241	41.30
mP20	713.44	402.81	1017.02	0.262	33.57
oP10	723.43	399.79	1012.80	0.267	32.59
tP15	720.76	370.91	949.81	0.280	28.50
rH15	736.85	534.69	1291.65	0.208	54.57

For assessing the brittle behavior and ductile behavior of crystal, Poisson's ratio ν is used as a quantitative index for distinguishing them, here the value of ν is taken to be 0.333, and the hP20 has the largest ν value of 0.342, beyond the threshold, suggesting that its ductility is better than others. The cP30 has the second largest ν value of 0.330, which is very close to

the threshold. The others, except cP20, all have superhard nature and their Poisson's ratio ν values are all smaller than that of po, which illustrates that they are brittle.

High pressure can significantly affect the mechanical properties of materials, hence we also calculate the elastic constants of these B_4C polymorphs at high pressures as 100 GPa and 150 GPa which satisfy the stability under pressure based on the phonon vibration analysis above. As shown in Table S3 and Table 2, of all the B_4C polymorphs under study, the rH15 has the largest mechanical moduli (B, G, E) and hardness. The smallest Poisson's ratio also indicates that rH15 is a brittle material. Compared with these mechanical properties obtained at ambient pressure and high pressure (100/150 GPa), the mechanical moduli (B, G, E) of all B_4C polymorphs increase with pressure increasing, while their hardness all decrease, which indicates that all B_4C polymorphs turn softer. This is consistent with the variation trend of Poisson's ratio, which has an increase trend with pressure increasing and suggests that the material becomes more ductile. Among all the B_4C polymorphs mentioned above, the mC10 is the one that stands out with an excellent ability of hardness maintained. The newly discovered B_4C polymorphs notably improves the mechanical properties of B_4C and enriches the industrial applications of B_4C.

3.5. Electronic properties

Based on the GGA, the electronic band structure of po-B_4C at ambient pressure is studied to analyze its electrical properties. The calculated band structure is replotted and displayed in Fig. 3(a). It is apparent that the valence band maximum (VBM) and conduction band minimum (CBM) are separated by a forbidden band with a gap of 2.832 eV. Also the highest value of valence band is located at G point, while the lowest value of conduction band is situated at Z point. Hence, the po-B_4C is an indirect gap semiconductor. It is considered that the calculation based on the GGA may underestimate the gaps.[56,57] Therefore, an exact hybrid functional HES06 is adopted. It is obvious that po-B_4C is an indirect gap semiconductor with a larger gap of 3.822 eV than that calculated by GGA, which is in good agreement with 4.13 eV reported by Ektarawong *et al.*[58]

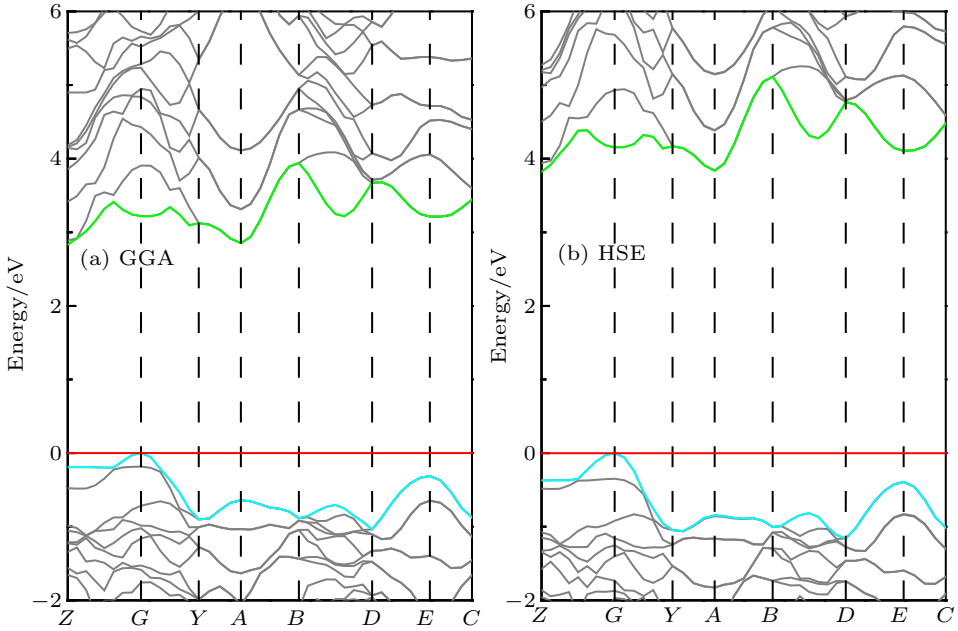

Fig. 3. Calculated band structure for (a) po-B_4C: GGA and (b) HSE06, with horizontal red line, cyan line, and green line representing Fermi level, VMB, and CMB, respectively.

Consider the fact that the gaps calculated by GGA are underestimated,[56,57] the accurate band structures of various B_4C polymorphs at ambient pressure are calculated based on the hybrid functional HSE06,[42] and the results are shown in Fig. 4. All but for the tP15 and cP20 possess metallicity. For mC10, hP20, and cP30, VBM, and CBM overlap to a certain extent near the Fermi level, while none of the aP10, mP20 and oP10 has any overlap between VBM and CBM, but their VBM and CBM cross the Fermi level. As for tP15 and cP20, their VBM and CBM are separated by band gap. Since neither of the highest value of valence band and the lowest one of conduction band is at the same highly symmetric point, they are both indirect bandgap semiconductors, respectively, with a gap of 0.910 eV and 1.314 eV.

Based on the HSE06, the partial densities of states (PDOSs) of these conductive phases including aP10, mC10, mP20, oP10, hP20, and cP30 are explored and exhibited in Fig. 5. It can be seen from the PDOS that all these B_4C polymorphs are indeed conductive due to the obvious electrons existing at the Fermi level. Through the PDOS analysis about

all the nonequivalent atoms listed in Table S1, all these polymorphs are identified to possess electrical conductivity in three dimensions due to all different species of atoms contributing to the electrons at the Fermi level.

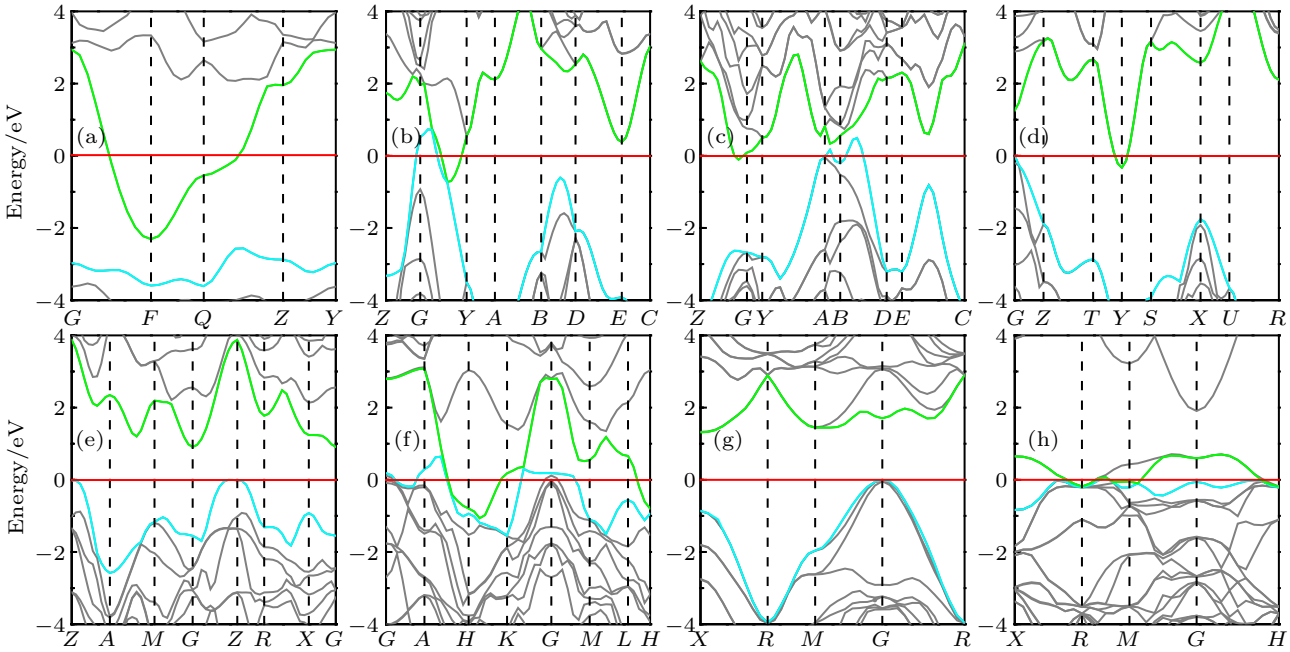

Fig. 4. Calculated band structures for B_4C models based on HSE06: (a) aP10, (b) mC10, (c) mP20, (d) oP10, (e) tP15, (f) hP20, (g) cP20, and (h) cP30, with horizontal red line, cyan line, and green line representing Fermi level, VMB, and CMB, respectively.

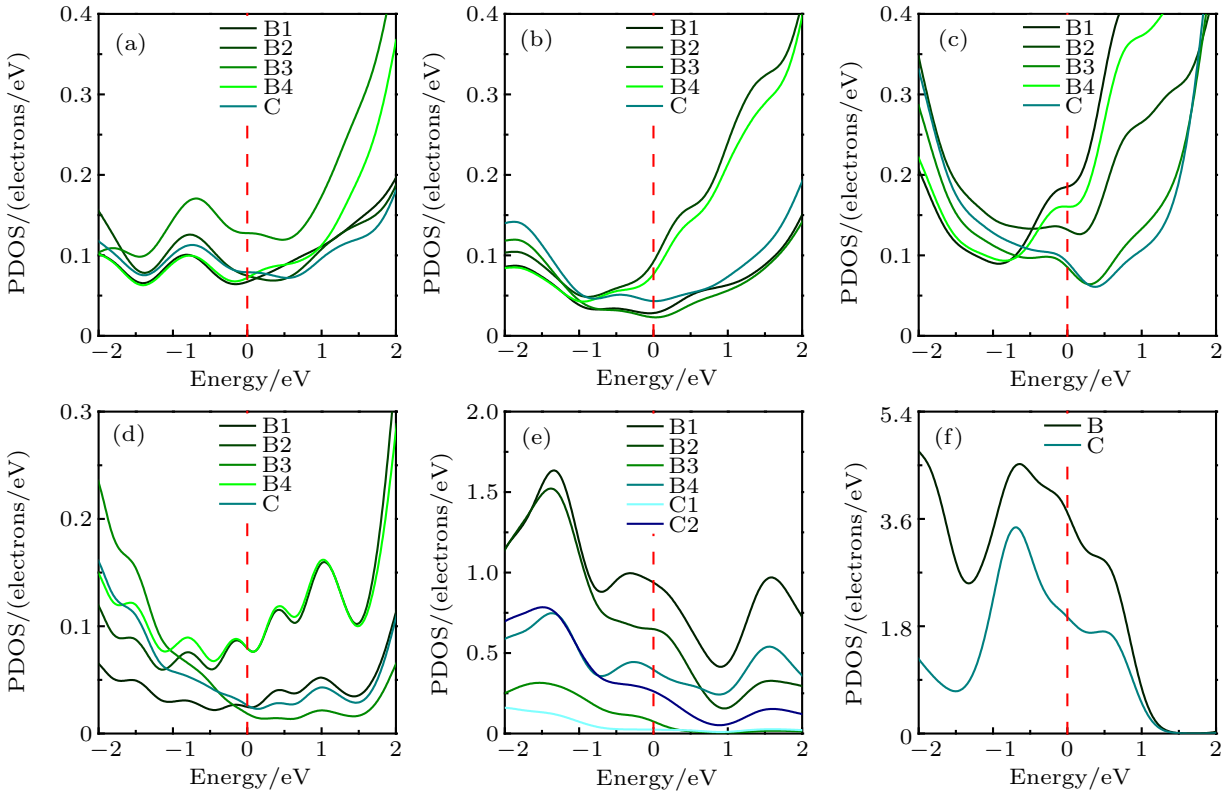

Fig. 5. Calculated PDOSs for B_4C models based on HSE06: (a) aP10, (b) mC10, (c) mP20, (d) oP10, (e) hP20, and (f) cP30, with red dash line denoting Fermi level.

Here, the oP10 istaken for example, the PDOSs of the five kinds of atoms (C, B1, B2, B3, and B4, Fig. 5(d) are calculated to analyze the origin of the metallic conductivity. It is obvious that the electrical conductivity is contributed by all of B4 and B2 atoms with rival electrons at Fermi level. While the B3, B1, and C atoms all contribute the conductive electrons far less than B4 and B2 atoms (no more than one-third of them) in the conducting behavior.

Further, electron orbital calculations are carried out to confirm the conductive directions in the oP10-B_4C, and the

calculated electron orbitals are obtained from the summation of the electronic bands across the Fermi level. As displayed in Fig. 6, the electron orbitals around all the atoms in the five-atom unit overlap. Whatever the directions including the [100], [010], and [001], the electron orbitals near the Fermi level are connected, indicating the conductive along the three-dimensional metallicity in the oP10-B_4C.

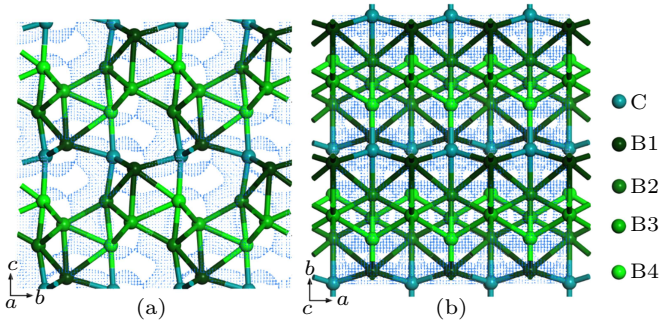

Fig. 6. Orbits near Fermi-level of oP10-B_4C at ambient pressure, viewing along axis (a) *a* and (b) *c*, respectively, with isovalue being 0.02 e/Å^3.

The physical performances of materials are heavily influenced by pressure. Conductivity is generally expected for most of semiconductors at high pressures because atoms are closely packed and the electron overlap will increase, so that the electron will no longer belong to a single atom nor a bond at this time. In other words, the so-called delocalization electron is formed, which means that the band gap is reduced and even metallized. According to the classical band theory, under the action of high pressure, the lattice parameters become smaller, the Brillouin region becomes larger, and the band widening results in the band gap decreasing. A typical case is metallic hydrogen.[59]

It is a very painful and tremendous timeconsuming job to calculate the accurate band structures based on HSE06, hence all the B_4C polymorphs are selected to calculate their band gaps under different pressures by the GGA method. Also the electron band structure at normal pressure is investigated based on GGA, and the results are presented in Fig. S6. Comparing the band structures acquired by GGA and HSE06, we find that there is no other difference except the sole difference in the band gap underestimation. For the tP15 it has a gap of 0.211 eV, and for the cP20 it has a gap of 0.569 eV, which are both significantly lower than the calculated values based on HSE06.

The relationship of bandgaps with pressure is obtained and plotted in Fig. S7. For tP15 and cP20, they both experience the process of the band gap decreasing. As pressure reaches 25GPa, the tP15 will lose its band gap, with the highest VB and the lowest CB both equaling zero. And the cP20 will become metallically conductive due to both the highest VB increase and the lowest CB decreasing to the Fermi level once pressure rises to 87.5 GPa. Then with the pressure increasing, both tP15 and cP20 keep metallically conductive. Their relationship of bandgaps with pressure accords with the common trends mentioned above.

4. Conclusions

In this work, we propose several B_4C polymorphs including a metastable phase of B_4C with icosahedra (cP30) and a series of B_4C high pressure phases with non-icosahedra. The B_4C high pressure phase (*e.g.*, mC10) is the postB_4C whose structure is transformed due to icosahedra being broken, and may be obtained through the HPHT. By studying mechanical properties, wefind that up to now, the cP30 is the most ductile B_4C structure, mC10, aP10, and tP15 are three hardest structures with superhard nature. The study of electrical properties-reveals that the cP20 and tP15 are both semiconductors with smaller indirect gaps and the other new B_4C structures possess metallicity. Under pressure, all B4C polymorphs except aP10 tend to be conductive (ch, eq, po, cP20, and tP15) or keep their original electrical conductivity values (mC10, mP20, oP20, hP20, and cP30) in the pressure range we studied. The gap of aP10 increases with pressure increasing, similar to an insulated sodium appearing due to high pressure compression. For the superhard B_4C, an accurate hybrid functional is employed to analyze the electronic band structure. The aP10 and tP15 are both indirect gap semiconductors and mC10 is metal with three dimensional conductivity. As the most stable phase of high pressure, mC10 has excellent ability to maintain hardness. We hope that our research will enrich the cognition of high pressure structural deformation of B_4C.

Acknowledgment

High-performance computational resources provided by the National Supercomputer Center on TianHe-2 in LvLiang Cloud Computing Center are also gratefully acknowledged.

References

[1] Domnich V, Reynaud S, Haber R A and Chhowalla M 2011 *J. Am. Ceram. Soc.* **94** 3605
[2] Liu M L, Liu C, Kumar U P and Chen M W 2020 *Mater. Res. Exp.* **7** 015904
[3] Vargas-Gonzalez L, Speyer R F and Campbell J 2010 *Int. J. Appl. Ceram. Tec.* **7** 643
[4] Wang C C and Song L L 2019 *Chin. Phys. B* **28** 066201
[5] Moshtaghioun B M, Cumbrera-Hernández F L, Gómez-García D, Bernardi-Martín S, Domínguez-Rodríguez A, Monshi A and Abbasi M H 2013 *J. Eur. Ceram. Soc.* **33** 361
[6] Johnson G R and Holmquist T J 1999 *J. Appl. Phys.* **85** 8060
[7] Zorzi J E, Perottoni C A and Jornada J A H 2005 *Mater. Lett.* **59** 2932
[8] Chen M W, McCauley J W and Hemker K J 2003 *Science* **299** 1563
[9] Shen Y, Li G and An Q 2019 *Scripta Mater.* **162** 306
[10] Orphal D L, Franzen R R, Charters A C, Menna T L and Piekutowski A J 1997 *Int. J. Impact Eng.* **19** 15
[11] Awasthi A P and Subhash G 2019 *J. Appl. Phys.* **125** 215901
[12] Yang X K, Coleman S P, Lasalvia J C, Goddard W A and An Q 2018 *ACS Appl. Mater. Inter.* **10** 5072
[13] Vogler T, Reinhart W and Chhabildas L 2004 *J. Appl. Phys.* **95** 4173

[14] Zhang Y, Mashimo T, Uemura Y, Uchino M, Kodama M, Shibata K, Fukuoka K, Kikuchi M, Kobayashi T and Sekine T 2006 *J. Appl. Phys.* **100** 113536

[15] Fanchini G, McCauley J W and Chhowalla M 2006 *Phys. Rev. Lett.* **97** 035502

[16] Mashimo T and Uchino M 1997 *J. Appl. Phys.* **81** 7064

[17] Zhao S T, Kad B, Remington B A, LaSalvia J C, Wehrenberg C E, Behler K D and Meyers M A 2016 *Proc. Natl. Acad. Sci. USA* **113** 12088

[18] Fujii T, Mori Y, Hyodo H and Kimura K 2010 *J. Phys. Conf. Ser.* **215** 012011

[19] Guo J J, Zhang L, Fujita T, Goto T and Chen M W 2010 *Phys. Rev. B* **81** 060102

[20] Dera P, Manghnani M H, Hushur A, Hu Y and Tkachev S 2014 *J. Solid State Chem.* **215** 85

[21] Kumar R S, Dandekar D, Leithe-Jasper A, Tanaka T, Xiao Y, Chow P, Nicol M F and Cornelius A L 2010 *Diam. Relat. Mater.* **19** 530

[22] Yan X Q, Tang Z, Zhang L, Guo J J, Jin C Q, Zhang Y, Goto T, McCauley J and Chen M W 2009 *Phys. Rev. Lett.* **102** 075505

[23] Domnich V, Gogotsi Y, Trenary M and Tanaka T 2002 *Appl. Phys. Lett.* **81** 3783

[24] Ge D, Domnich V, Juliano T, Stach E and Gogotsi Y 2004 *Acta Mater.* **52** 3921

[25] Yan X Q, Li W J, Goto T and Chen M W 2006 *Appl. Phys. Lett.* **88** 131905

[26] Ghosh D, Subhash G, Lee C H and Yap Y K 2007 *Appl. Phys. Lett.* **91** 061910

[27] Lazzari R, Vast N, Besson J, Baroni S and Dal Corso A 1999 *Phys. Rev. Lett.* **83** 3230

[28] Reddy K M, Liu P, Hirata A, Fujita T and Chen M W 2013 *Nat. Commun.* **4** 2483

[29] Xie K Y, An Q, Sato T, Breen A J, Ringer S P, Goddard W A, Cairney J M and Hemker K J 2016 *Proc. Natl. Acad. Sci. USA* **113** 12012

[30] An Q, Goddard W A and Cheng T 2014 *Phys. Rev. Lett.* **113** 095501

[31] Li J, Xu S, Zhang J Y, Liu L S, Liu Q W, She W C and Fu Z Y 2017 *Chin. Phys. B* **26** 047101

[32] Aryal S, Rulis P and Ching W Y 2011 *Phys. Rev. B* **84** 184112

[33] An Q and Goddard W A 2015 *Phys. Rev. Lett.* **115** 105501

[34] Korotaev P, Pokatashkin P and Yanilkin A 2015 *Modell. Simul. Mater. Sci. Eng.* **24** 015004

[35] Korotaev P, Pokatashkin P and Yanilkin A 2016 *Comput. Mater. Sci.* **121** 106

[36] Xinxin Z, Yu Z, Miao Z, Hanyu L, Yansun Y, Taimin C and Hui C 2017 *J. Phys.: Condens. Matter* **29** 455401

[37] Wang Y C, Lv J A, Zhu L and Ma Y M 2010 *Phys. Rev. B* **82** 094116

[38] Zhao Z S, Tian F, Dong X, Li Q, Wang Q Q, Wang H, Zhong X, Xu B, Yu D L, He J L, Wang H T, Ma Y M and Tian Y J 2012 *J. Am. Chem. Soc.* **134** 12362

[39] Zhang S S, He J L, Zhao Z S, Yu D L and Tian Y J 2019 *Chin. Phys. B* **28** 106104

[40] Clark S J, Segall M D, Pickard C J, Hasnip P J, Probert M I J, Refson K and Payne M C 2005 *Z. Kristallogr.* **220** 567

[41] Perdew J P, Ruzsinszky A, Csonka G I, Vydrov O A, Scuseria G E, Constantin L A, Zhou X and Burke K 2008 *Phys. Rev. Lett.* **100** 136406

[42] Krukau A V, Vydrov O A, Izmaylov A F and Scuseria G E 2006 *J. Chem. Phys.* **125** 224106

[43] Adenwalla S, Welsch P, Harken A, Brand J, Sezer A and Robertson B W 2001 *Appl. Phys. Lett.* **79** 4357

[44] Vast N, Lazzari R, Besson J, Baroni S and Dal Corso A 2000 *Comput. Mater. Sci.* **17** 127

[45] Vast N, Sjakste J and Betranhandy E 2009 *J. Phys. Conf. Ser.* **176** 012002

[46] Fujimori M, Nakata T, Nakayama T, Nishibori E, Kimura K, Takata M and Sakata M 1999 *Phys. Rev. Lett.* **82** 4452

[47] Mouhat F and Coudert F 2014 *Phys. Rev. B* **90** 224104

[48] Oganov A R, Chen J, Gatti C, Ma Y, Ma Y, Glass C W, Liu Z, Yu T, Kurakevych O O and Solozhenko V L 2009 *Nature* **457** 863

[49] Zarechnaya E Y, Dubrovinsky L, Dubrovinskaia N, Miyajima N, Filinchuk Y, Chernyshov D and Dmitriev V 2008 *Sci. Tech. Ad. Mater.* **9** 044209

[50] Haussermann U, Simak S I, Ahuja R and Johansson B 2003 *Phys. Rev. Lett.* **90** 065701

[51] Solozhenko V L, Kurakevych O O, Andrault D, Le Godec Y and Mezouar M 2009 *Phys. Rev. Lett.* **102** 015506

[52] Mannix A J, Zhou X-F, Kiraly B, Wood J D, Alducin D, Myers B D, Liu X, Fisher B L, Santiago U and Guest J R 2015 *Science* **350** 1513

[53] Wu Z, Zhao E, Xiang H, Hao X, Liu X and Meng J 2007 *Phys. Rev. B* **76** 054115

[54] Chen X Q, Niu H Y, Li D Z and Li Y Y 2011 *Intermetallics* **19** 1275

[55] Tian Y J, Xu B and Zhao Z S 2012 *Int. J. Refract. Met. H.* **33** 93

[56] Xiao H, Tahir-Kheli J and Goddard W A 2011 *J. Phys. Chem. Lett.* **2** 212

[57] Garza A J and Scuseria G E 2016 *J. Phys. Chem. Lett.* **7** 4165

[58] Ektarawong A, Simak S, Hultman L, Birch J and Alling B 2014 *Phys. Rev. B* **90** 024204

[59] Dias R P and Silvera I F 2017 *Science* **355** 715